SUPPORTING INFORMATION

Content

1. Experimental Details – Materials and General Methods

All used reagents and solvents were purchased from commercial sources. Unless otherwise noted, all manipulations were carried out under a dry nitrogen or argon atmosphere. Solvents were degassed prior to use with four freeze-pump-thaw cycles and were stored in sealed Schlenk ampulla over activated molecular sieve (3 or 4 Å, respectively) under a dry argon atmosphere. Liquid reactants were degassed for at least 10 min with a constant stream of dry argon through the fluid phase and were dried by storage over activated molecular sieve (3 or 4 Å, respectively). Solid reagents were dried and purified if necessary either by the application of *vacuum* and elevated temperature, or by sublimation under reduced pressure at elevated temperature.

All reactions on preparative scale were carried out in flame-dried standard laboratory glassware under a dry argon atmosphere using Schlenk line techniques and were permanently magnetically stirred. Syringes, magnetic stirring bars, and needles were dried and/or flushed with argon prior to use. Reactions on the NMR sample scale were done in dry *J. Young* NMR tubes. Compounds sensitive to ambient conditions were handled and stored in a *Sylatech* glove box filled with dry nitrogen gas. Removal of solvents in *vacuo* was performed using a *Heidolph VV2000* rotary evaporator or a Schlenk line. Literature-known compounds were synthesized following published procedures, which are cited (see below).

Nuclear magnetic resonance (NMR) spectra were collected with a *Bruker BZH 200/52*, a *Bruker DPX 200*, a *Bruker Avance II 400*, a *Bruker Avance III 500* or a *Bruker Avance III 600* spectrometer at 298 K unless otherwise noted. Measurements with the *Bruker Avance* spectrometers were carried out by the NMR facilities of the Institutes of Inorganic or Organic Chemistry of the Heidelberg University.

Chemical shifts δ are given in parts per million (ppm) relative to the tetramethylsilane resonance. Deuterated dichloromethane and chloroform were used as solvent, and the signal of $CHDCl_2$ or $CHCl_3$ was used for calibration of the spectra (CD_2Cl_2: ^{1}H: 5.32 ppm, ^{13}C: 53.84 ppm, $CDCl_3$: ^{1}H: 7.26 ppm, ^{13}C: 77.16 ppm, toluene-*d8*: ^{1}H: 2.08 ppm, ^{13}C: 20.43 ppm). Spectra in *ortho*-difluorobenzene (*o*-$C_6H_4F_2$) were obtained after the addition of C_6D_6 or without lock. The signals obtained *o*-$C_6H_4F_2$ samples were not internally referenced and reported as received. ^{1}H and ^{19}F NMR data is reported as follows: chemical shift δ [ppm], multiplicity (s = singlet, br = broad singlet, d = doublet, t = triplet, q = quartet, quin = quintet, sext = sextet, sept = septet, m = multiplet, and combinations), scalar spin-spin coupling constant [Hz] as $^XJ_{AB}$ (X = number of chemical bonds between coupled nuclei; A, B = coupled nuclei), integration value. ^{13}C, ^{29}Si and ^{31}P NMR data are reported as follows: chemical shift δ [ppm], multiplicity (if apparent), scalar spin-spin coupling constant [Hz] as $^XJ_{AB}$. NMR spectra were processed and plotted with *MestReNova 14.2*.

High resolution mass spectrometry (HR-MS) was conducted with the electrospray ionization method (ESI) on a *Bruker ApexQe hybrid 9.4 T FT-ICR* or with electron impact ionization (EI) on a *JEOL JMS-700* magnetic sector, carried out by the Mass Spectrometry Facility of the Institute of Organic Chemistry of Heidelberg University. Mass spectrometry data is reported as follows: *m/z* ratio (relative intensity) [assigned fragment] (for HR experiments: calculated exact mass).

Gas chromatography mass spectrometry (GCMS) experiments were conducted utilizing helium as carrier gas on a *Thermo Fischer Scientific Ultra Trace* gas chromatograph equipped with a *TraceGOLD TG-1701MS* column (14% cyanopropylphenyl, 86% dimethylpolysiloxane, 30 m x 0.25 mm x 0.25 μm) and a *Thermo Fischer Scientific ISQ Single Quadropole* Mass Selective Detector. Unless stated otherwise, the following column program was used: at a constant pressure of 50 kPa the initial temperature of 35 °C was held for 5 min after injection, then increased by 30 K/min to 250 °C, this temperature kept for 10 min before cooling to 150 °C at a rate of 25 K/min. Reported retention times refer to this program.

IR spectra were measured on a *Bruker Alpha* or an *Agilent Cary 630* spectrometer equipped with diamond ATR units. IR spectra were processed and plotted with *OriginPro 2021 (9.8.0.200)*.

Electrochemical measurements were performed with a potentiostat (EmStat3+ Blue, PalmSens Compact Electrochemical Interfaces) in a *SylaTech* glovebox under nitrogen atmosphere in a glass cell using a three-electrode configuration. A glassy carbon electrode with a working area of 0.07 cm^2, was used as working electrode, a platinic wire as counter electrode; a silver wire served as quasi reference electrode. The program *PSTrace 5.9* was used to record all measurements. The substances were examined at room temperature with the electrolyte [N*n*Bu$_4$][PF$_6$] (c = 0.1 M, V = 5 mL) in dichloromethane at a scan rate of 50 mV/s, unless otherwise stated. The solutions were stirred between each measurement and kept under nitrogen atmosphere throughout. As internal standard ferrocene was measured at the very end of the measurement.

X-band EPR measurements (9.30-9.55 GHz) were conducted at room temperature on a *MiniScope MS400* (magenettech) spectrometer with a modulation frequency of 100 kHz.

2. Syntheses

3,6-di-*tert*-butyl-catechol

The preparation of the compound was guided by *Ershov's* protocol.[1] In absence of an autoclave and guided by literature known procedures,[2, 3] the reaction was carried out in a thick-walled Schlenk-ampulla and isobutene was applied to the reaction mixture as liquid at low temperatures. The altered setup resulted in lower yields, presumably associated with reduced pressure.

¹H NMR (200 MHz, CDCl$_3$) δ 6.77 (s, 2H, C*H*), 5.36 (s, 2H, O*H*), 1.41 (s, 18H, C*H*$_3$).
¹³C NMR (101 MHz, CDCl$_3$) δ 143.3 (*C*$_{Ar}$O), 134.3 (*C*$_{Ar}$^{t}C$_4$H$_9$), 117.6 (*C*$_{Ar}$H), 34.1 (*C*$_q$(CH$_3$)$_3$), 30.0 (*C*H$_3$).

GCMS EI+ 12.9 min. m/z 222.3 [M]$^+$ (24%), 207.4 [M – CH$_3$]$^+$ (100%).

Bis(3,6-di-tert-butyl-catecholato)silane (1)

To a solution of 3,6-di-*tert*-butyl-catechol (2.0 eq.) in acetonitrile (0.2 M) HSiCl$_3$ (1.0 eq.) was added slowly. The mixture was stirred at rt overnight while ensuring a continuous exchange of the inert atmosphere. The formed colorless precipitate was filtered, washed with acetonitrile, and dried in *vacuo*, to yield a colorless solid (1.3 g, 82%).
Crystals suitable for scXRD were grown by liquid diffusion of acetonitrile into a solution of the title compound in dichloromethane.

¹H NMR (600 MHz, CDCl$_3$) δ 6.90 (s, 4H, C$_{Ar}$*H*), 1.40 (s, 36H, C(C*H*$_3$)$_3$).
¹³C NMR (151 MHz, CDCl$_3$) δ 144.9 (*C*$_{Ar}$O), 134.4 (*C*$_{Ar}$C$_4$H$_9$), 119.2 (*C*$_{Ar}$H), 34.3 (*C*$_q$(CH$_3$)$_3$), 29.6 (*C*H$_3$).
²⁹Si NMR (119 MHz, CDCl$_3$) δ −42.9.

HRMS EI+ (*m/z*) calc. for [C$_{28}$H$_{40}$O$_4$Si]$^+$ [M]$^+$, 468.2690; found 468.2704 (23%), deviation 2.91 ppm; calc. for [C$_{27}$H$_{37}$O$_4$Si]$^+$ [M–CH$_3$]$^+$, 453.2456; found 453.2466 (100%), deviation 2.33 ppm.

Elemental Analysis calc. C: 71.75 H: 8.60 found: C: 71.80 H: 8.55.

IR (ATR-FTIR): ṽ [cm^{-1}] 2990 (w, ν^{CH}), 2957 (m, ν^{CH}), 2909 (w, ν^{CH}), 2870 (w, ν^{CH}), 1559 (w), 1501 (m), 1483 (m), 1468 (m), 1395 (m, δ^{tBu}), 1386 (s, δ^{tBu}), 1359 (m), 1315 (m), 1286 (m), 1226 (s), 1204 (m), 1140 (m), 1206 (m), 999 (s), 966 (m).

[1][B(C₆F₅)₄]

[N(p-C₆H₄Br)₃][B(C₆F₅)₄][4] (1.00 eq.) was added to a solution of **1** (1.05 eq.) in *ortho*-difluorobenzene (0.05 M). The mixture was stirred for 10 d at rt, during which the solution turned continuously more intense dark, moss green to brown from an initial deep blue color. The mixture was concentrated in *vacuo* and the remaining viscous triturated with *n*-hexane. The resulting dark solid flakes were filtered off, powdered, and washed with *n*-hexane (x3 5 mL), to yield a deep dark green to blue solid (234 mg, 75%).

General remarks on the characterization of [1][B(C₆F₅)₄]

The analytical characterization generally supported the formation of the **1**⁺• structural motif. Potential adduct-formation of **1**⁺• and N(p-C₆H₄Br)₃ could not be confirmed by any of the characterizations, which is in line with computations that reveal an endergonic process. Trace amounts of other paramagnetic species were indicated by minor deviation of EPR simulation and experiment (Correlation 99.3%, **Figure S4**). Fragments assignable to fluoride adduct species of **1**⁺• as well as to the extrusion of isobutene detected in the ESI mass spectrum supported the high reactivity and related limited stability of **1**⁺•. Minor reduced C and H proportions in the elemental analysis might be attributed to this elimination of isobutene ($-C_4H_8$) from the semiquinone system during combustion. Such pathways have been reported previously for related *tert*-butyl-phenol derivatives under oxidative conditions.[5, 6]

¹H NMR (600 MHz, *o*-C₆H₄F₂) δ 1.15 (s, 36H, C(C**H₃**)₃). C$_{Ar}$**H** was not detected.
¹¹B NMR (193 MHz, *o*-C₆H₄F₂) δ −16.3.
¹³C NMR (151 MHz, *o*-C₆H₄F₂) δ 31.0 (**C**H₃). **C**$_{Ar}$ and **C**(CH₃)₃ were not detected.
¹⁹F NMR (565 MHz, *o*-C₆H₄F₂) δ −132.4 (br, 2F), −163.4 (br, 1F), −167.2 (br, 2F).
²⁹Si NMR (119 MHz, *o*-C₆H₄F₂) No signal detected.

EPR (ν_x = 9.450515 GHz, *o*-C₆H₄F₂): g^{iso} = 2.00269 triplet with simulated $A_H{}^{iso}$ = 716 µT.

HRMS ESI+ in *o*-C₆H₄F₂ (*m/z*) calc. for [**1** + 2H + F]⁺, 489.2831; found 489.3188 (5%), deviation 73 ppm; calc. for [**1** + H + F − C₃H₆]⁺, 446.2284; found 446.2590 (21%), deviation 67 ppm; calc. for [**1** + H + F − C₄H₉]⁺, 432.2127; found 432.2434 (87%), deviation 71 ppm.

Elemental Analysis calc. C: 54.42 H: 3.51 found: C: 53.70 H: 2.89.

IR (ATR-FTIR): ṽ [cm⁻¹] 3179 (w, ν^{CH}), 3101 (w, ν^{CH}), 2963 (m, ν^{CH}), 2873 (w, ν^{CH}), 1643 (m), 1571 (br), 1511 (m), 1458 (s), 1375 (w, δ^{tBu}), 1272 (m), 1199 (w), 1167 (w), 1088 (s), 1013 (m), 974 (s).

3. Evaluation of the Dynamic Covalent Chemistry of Bis(alkyl-catecholato)silanes

As mentioned in the main text, within this work the alkylated bis(alkyl-catecholato)silanes bis(3,6-di-*tert*-butyl-catecholato)silane (Si(cat$^{3,6-tBu}$)$_2$, **1**), bis(3,6-tri-*iso*-propyl-catecholato)silane (Si(cat$^{3,4,6-iPr}$)$_2$), and bis(3,5-di-cumyl-catecholato)silane (Si(cat$^{3,5-Cm}$)$_2$) were evaluated regarding their dimerization behavior.

The ^{29}Si NMR spectroscopic data was compared with the computed resonances (see computational details, **Table S6**) which is illustrated in **Table S1**. For Si(cat$^{3,4,6-iPr}$)$_2$[7] and **1** single signals at −41.2 ppm and −42.9 ppm were detected, respectively. A comparison with structurally related bis(pinacolato)silane (δ(^{29}Si) = −44.4 ppm)[8] gave a first shallow indication for a similar coordination environment. Further evidence for a single entity was provided by the calculation of NMR resonances for the monomeric forms (Si(cat$^{3,4,6-iPr}$)$_2$: −38.8 ppm,[7] **1**: −38.9 ppm, see computational details). In contrast, calculated resonances for the corresponding dimers were in clear discrepancy to the experimentally obtained spectroscopic data (**Table S1**).

In the case of Si(cat$^{3,5-Cm}$)$_2$ four ^{29}Si NMR signals of different intensity are reported which was assigned to different diastereomers of the respective dimer [Si(cat$^{3,5-Cm}$)$_2$]$_2$ that was confirmed in the solid state by scXRD analysis.[9] A calculated ^{29}Si NMR shift based on the respective dimeric solid-state structure was in a fitting range to the experimentally obtained resonances, suggesting that the dimeric entity is also favored in solution. In contrast, the calculated shift for a putative monomer was in sharp disagreement. Absence of further up-field signals ruled the possibility of higher oligomeric forms unlikely.[9]

Table S1. Comparison of experimental and computed ^{29}Si NMR resonances of different bis(alkyl-catecholato)silanes.

Compound	Computed ^{29}Si NMR resonance(s) δ_{comp}(^{29}Si) [ppm]	Experimentally obtained ^{29}Si NMR resonance(s) δ_{exp}(^{29}Si) [ppm]
Bis(pinacolato)silane	-	−44.4[8]
Si(cat$^{3,6-tBu}$)$_2$ (**1**)	−38.9[a]	−42.9[b]
[Si(cat$^{3,6-tBu}$)$_2$]$_2$ ([**1**]$_2$)	−78.5[a] −77.9[a]	*n.d.*
Si(cat$^{3,4,6-iPr}$)$_2$	−38.8[a]	−41.1[7]
[Si(cat$^{3,4,6-iPr}$)$_2$]$_2$	−72.7[a] −66.1[a]	*n.d.*
Si(cat$^{3,5-Cm}$)$_2$	−38.9[a]	*n.d.*
[Si(cat$^{3,5-Cm}$)$_2$]$_2$	−69.2[a] −74.3[a]	−62.8, −71.2, −71.7, −71.9[9]

[a] this work, see section computational details; [b] this work, see experimental section.

For a better understanding on the relation of the ligand's substituents and the structure of the silicon species, the dimerization process of the silanes Si(cat$^{3,4,6-iPr}$)$_2$, **1**, and Si(cat$^{3,5-Cm}$)$_2$ was investigated computationally (see **Table S2**). For Si(cat$^{3,4,6-iPr}$)$_2$ and **1** the distorted tetrahedral, monomeric form was found to be thermodynamically favored in comparison to their respective dimers [Si(cat^R)$_2$]$_2$, matching the experimental observations. Similarly, in line with the spectroscopic data and its solid-state structure,[9] the cumyl substituted derivative Si(cat$^{3,5-Cm}$)$_2$ was predicted to dimerize.

Table S2. Illustration of the computed thermodynamic and kinetic data for the dimerization of different bis(alkyl-catecholato)silanes.

R	ΔG‡ [kJ mol^{-1}]	ΔG [kJ mol^{-1}]
3,4,6-^{i}Pr	+103	+56
3,6-^{t}Bu	+89	+21
3,5-cumyl	+38	−63

In similarity to the exceptionally low barriers calculated for the Si-O *sigma* bond metathesis of Si(cat)$_2$,[9] the here found transition state energies are comparably low (**ΔG‡**, **Table S2**). Based on these energies, a kinetic hindrance at room temperature cannot be disclosed. The computations overall support that the favoring of low-nuclearity entities of sterically congested bis(catecholato)silanes can in first regard subjected to a thermodynamic but not necessarily a kinetic inhibition. Moreover, a combined consideration of experiment and theory indicates a necessity for the substitution of both *ortho* positions as crucial for a thermodynamic prevention of self-aggregation.

4. Catalysis

A *J. Young* type NMR tube was charged with **x** mol% **catalyst**, **substrate(s)** and CD_2Cl_2 (0.4 mL). The reaction was conducted at rt and monitored using ^{1}H NMR spectroscopy. Cyclooctane was added as internal standard and yields were determined by integration. For details see **Table S3**. Spectra for the catalytic COM and respective control experiments are illustrated in **Figure S1**. Spectra for the Friedel-Craft's Dimerization and the dihydrodeoxygenation reactions are illustrated in **Figure S12**.

Products were characterized *via* NMR spectroscopy and verified by comparison with literature characterization data, which are listed below along with the respective references.

1-methyl-1,3,3-triphenyl-2,3-dihydro-1H-indene.[10]
^{1}H NMR (600 MHz, CDCl$_3$): δ 7.40 – 7.12 (m, 20H), 3.50 (d, J = 13.6 Hz, 1H), 3.20 (d, J = 13.6 Hz, 1H), 1.64 (s, 3H).
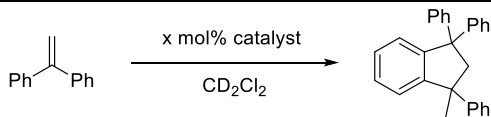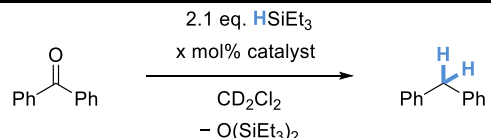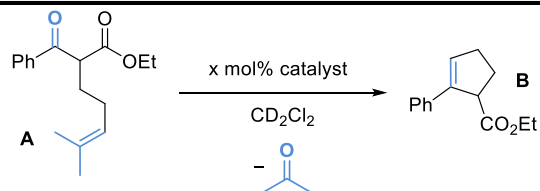
Diphenylmethane.[11, 12]
^{1}H NMR (200 MHz, CD$_2$Cl$_2$) δ 7.42 – 7.14 (m, 10H), 4.01 (s, 2H).

**Ethyl 2-phenylcyclopent-2-ene-1-carboxylate (B).**[12, 13]
^{1}H NMR (600 MHz, CD$_2$Cl$_2$) δ 7.45 – 7.40 (m, 2H), 7.34 – 7.27 (m, 2H), 7.25 – 7.19 (m, 1H), 6.36 (td, J_{HH} = 2.6, 1.6 Hz, 1H), 4.13 – 4.00 (m, 2H), 3.96 (m, 1H), 2.68 (m, 1H), 2.60 – 2.50 (m, 1H), 2.36 (dtd, J_{HH} = 13.0, 9.2, 6.6 Hz, 1H), 2.25 – 2.15 (m, 2H), 1.15 (t, $^3J_{HH}$ = 7.1 Hz, 3H).

Table S3. Details on the catalytic procedures.

Substrate(s)	Catalyst	x	t [h]	Yield [%]
1,1-diphenylethylene (100 µmol)				
	[1][B(C$_6$F$_5$)$_4$]	2.5	5	94%
benzophenone (50 µmol) & HSiEt$_3$ (105 µmol)				
	[1][B(C$_6$F$_5$)$_4$]	5	1	93%
			5	95%
	1	5	24	n.d.
	[N(p-C$_6$H$_4$Br)$_3$][SbCl$_6$]	5	14	n.d.
A (50 µmol)				
	[1][B(C$_6$F$_5$)$_4$]	5	1	> 97%
	1	5	14	n.d.
	[N(p-C$_6$H$_4$Br)$_3$][SbCl$_6$]	5	14	n.d.
	1 & [N(p-C$_6$H$_4$Br)$_3$][B(C$_6$F$_5$)$_4$]	5*	1	> 97%

* 5 mol % of silane and oxidant were mixed in CD$_2$Cl$_2$ and allowed to react for approx. 1 min. **prior** to addition of substrate and internal standard.
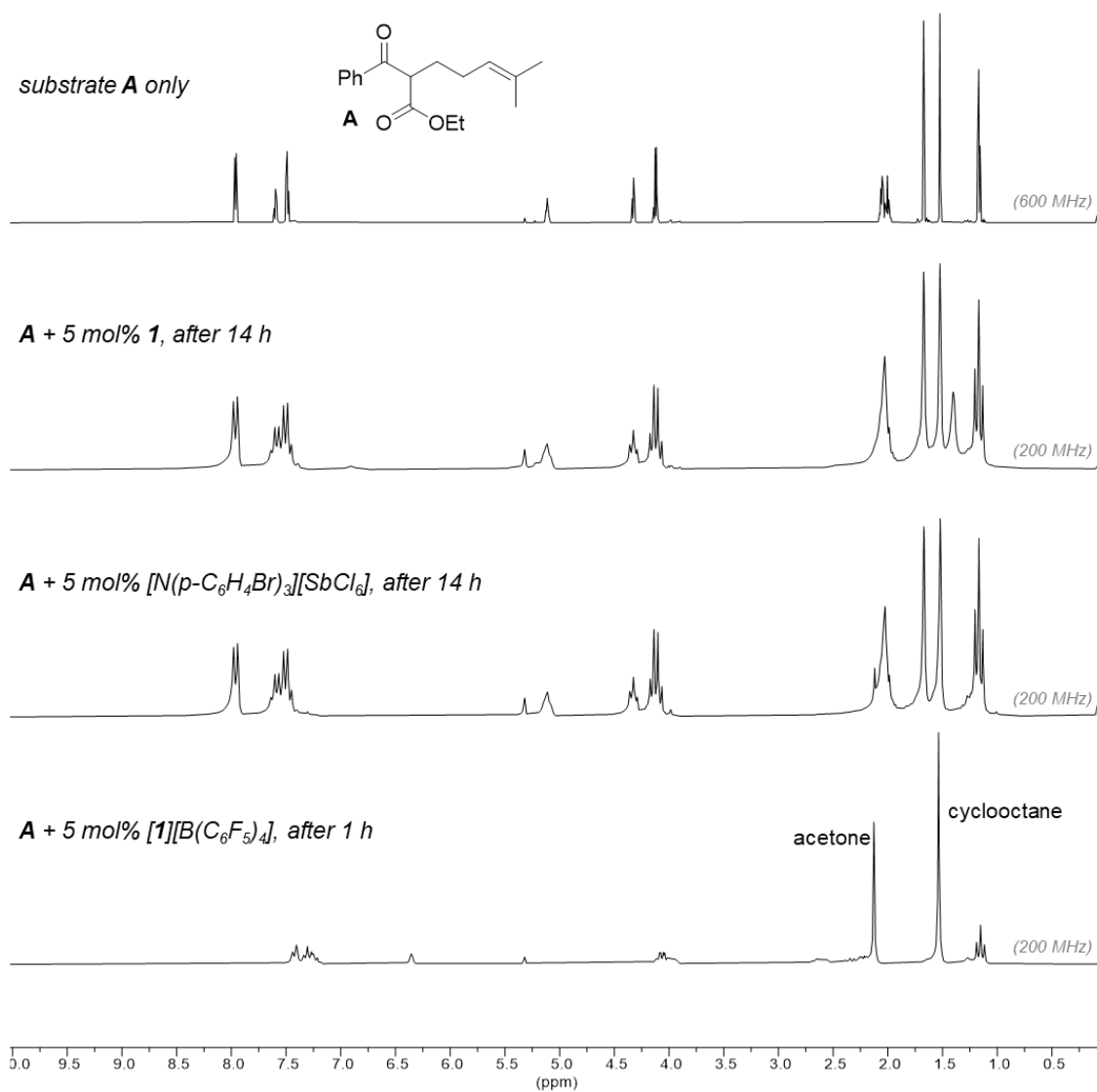
Figure S1. Stacked ^{1}H NMR spectra (in CD_2Cl_2) for the COM substrate **A,** the control experiments with **A** and **1** as well as with **A** and [N(p-$C_6H_4Br)_3$][SbCl$_6$] and the spectrum of the reaction mixture of **A** and [**1**][B($C_6F_5)_4$] after 1 h.

5. Computational Details

General Remarks

Unless stated otherwise, all computations were processed using the *Orca* 4.2 or 5.0 program package,[14, 15] in part extended by the GFN-xTB methods provided in the corresponding software package.[16-18] As initial guess, VSEPR structures preoptimized with force-field methods in the *Avogadro*[19] software were used. In general, these starting structures were directly applied for the optimization.

The resolution-of-identity[21] and "chain of spheres"[22] approximation in the form of RIJCOSX was used in combination with matching auxiliary basis sets.[23] When applied, the *Becke-Johnson* damping function[24, 25] in conjunction with *Grimme's* semi-empirical dispersion correction[26, 27] is denoted as *D3(BJ)*. The physically improved and more sophisticated successor model is denoted as *D4*.[28] Calculations incorporated the GFN2-xTB method (xTB2),[17] the composite schemes PBEh-3c[29] and r^{2}SCAN-3c,[30] the PBE0,[31, 32] PW6B95,[33] and DSD-BLYP[34] functionals, the basis sets def2-TZVPP,[35, 36] def2-QZVPP,[35, 36] aug-cc-pVQZ,[37-42] and cc-pVDZ.[37-42] Additionally, the DLPNO-CCSD(T)[43-45] method was utilized for obtaining single point energies. Solvation corrections incorporated the conductor-like polarizable continuum model (CPCM), the analytical linearized Poisson–Boltzmann model (ALPB)[46] or the *Universal Solvent Model* (SMD).[47] A concentration term of $\Delta G_{conc} = RT\ln(24.5) = 7.9$ kJ mol^{-1} (298 K) for the solution Gibbs free energy was additionally considered, arising from a change of gas (1 atm) to solution phase (1 M).[48] Used combinations of schemes, functionals, basis sets, and solvation models are denoted respectively.

Thermodynamic data at 298 K were computed using the rigid-rotor harmonic oscillator (RRHO) approximation at the level of optimization.[49] Calculated structures have been confirmed as energetic minima on the potential energy surface by the analytical calculation of harmonic frequencies. Transition geometries were optimized toward a single negative Hessian matrix eigenvalue. It was ensured that the correct first-order saddle point on the potential energy surface was located by animation of the imaginary frequency.[50] For the structures TS-[Si(cat$^{3,5\text{-}Cm}$)$_2$]$_2$‡ and [Si(cat$^{3,4,6\text{-}iPr}$)$_2$]$_2$ one additional imaginary mode was encountered (value < 10 cm^{-1}), which was respectively judged to be artificial after visualization. The artificial imaginary modes were treated as infinitesimal positive, and the respective Gibbs free energies thus manually corrected by −11.2 kJ mol^{-1} per mode, according to *Grimme's* quasi-RRHO approach.[49]

Resulting energies, anion affinities, thermodynamic and kinetic data, as well as computed NMR resonances are summarized in **Tables S4-S8**.

Anion Affinities

Single point energies of optimized structures were obtained at the DLPNO-CCSD(T) level of theory in conjunction with the def2-QZVPP basis set. Final anion affinities were determined according to the protocol proposed by *Krossing*,[51, 52] using an *iso*desmic reaction scheme against CCSD(T)/CBS anchor points.[53, 54]

Solvation correction for the anion affinities was considered as suggested in literature.[53, 54] To extract enthalpic contribution of solvation the following protocol was used. First, solvation free energies were obtained by COSMO-RS[55] in dichloromethane as implemented in ADF[56] based on BP86/TZP[57] single point energy calculations for the electrostatic solute-solvent interaction on the gas-phase structures.[58-61] Then, COSMO-RS correction for enthalpies was achieved by calculating ΔG-corrections at five different temperatures (278.15, 288.15, 298.15, 308.15, 318.15 K). A linear fit of satisfying $\Delta G = \Delta H - T\Delta S$ plots of the obtained Gibbs free energy corrections against the temperature allowed to extract the corrections for ΔH.

Calculation of NMR Resonances

Calculation of ^{29}Si NMR resonances was conducted at the PBE0-D3(BJ)+SMD(*solvent*)/def2-TZVPP level of theory, as this combination was shown to be a reliable method.[62] Solvation effects were considered implicitly, using the *Universal Solvent Model* (SMD).[47] Resonances were referenced against tetramethylsilane, for which optimization and chemical shielding were calculated in the same manner.

Natural bond orbital analysis

Natural bond orbital (NBO) analysis was conducted with the NBO7 software (NBO 7.0. E. D. Glendening, J. K. Badenhoop, A. E. Reed, J. E. Carpenter, J. A. Bohmann, C. M. Morales, P. Karafiloglou, C. R. Landis, and F. Weinhold, Theoretical Chemistry Institute, University of Wisconsin, Madison, WI (2018)), which is applicable within the Orca program package. The calculation was performed at the PBE0-D3(BJ)/def2-TZVPP+CPCM(CH$_2$Cl$_2$) level of theory. The respective spin-density plot is illustrated in **Figure S2**.
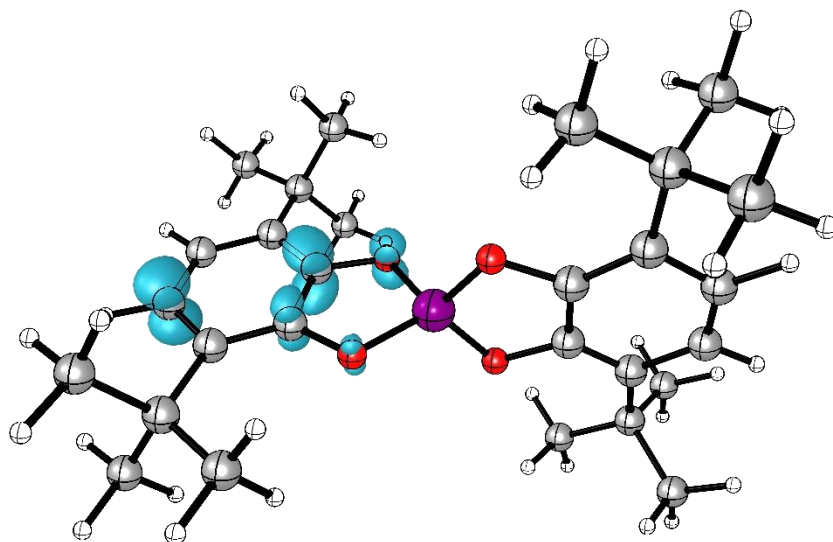
Figure S2. Computed spin-density distribution of **1**[•+] (isosurface threshold: 0.0175).

Table S4. Computed energies for the determination of *vacuum* fluoride ion affinities.

Compound	E^{OPT} [H]	H^{OPT} [H]	E^{SP} [H]	H_{tot} [kJ mol^{-1}]	FIA [kJ mol^{-1}]
Me₃Si$^{+[a]}$	-408.7706	-408.6530	-408.3655	-1071854.7	
Me₃SiF$^{[a]}$	-508.9244	-508.8018	-508.5046	-1334757.0	
1 $^{[a]}$	-1680.5301	-1679.8646	-1679.2498	-4407123.6	
[F-**1**]$^{-[a]}$	-1780.4803	-1779.8127	-1779.1771	-4669477.1	**403.7** (FIA)
1$^{•+[a]}$	-1680.2482	-1679.5847	-1678.9566	-4406358.9	
[F-**1**]$^{•[a]}$	-1780.3494	-1779.6812	-1779.0312	-4669092.2	**783.5** (FIA)
[F₂-**1**]$^{-•[a]}$	-1880.2617	-1879.5910	-1878.9302	-4931370.8	**328.8** (FIA)

FIA = −[ΔH(LA + Me₃SiF → Me₃Si$^+$ + LA-F) – anchor point]
Anchor point: 952.5 kJ mol^{-1} (FIA).[53]

[a] DLPNO-CCSD(T)/def2-QZVPP//PBE0-D3(BJ)/def2-TZVPP (*Orca 5.0*).

Table S5. Solvation corrected fluoride ion affinities.

Compound	ΔH$_{solv}$(CH₂Cl₂) [kJ mol^{-1}]	System	FIA/HIA (CH₂Cl₂) [kJ mol^{-1}]
F$^-$	−333.9		
1	-71.8		
[F-**1**]$^-$	-209.9	**1** / [F-**1**]$^-$	**201.9** (FIA)
[**1**]$^{•+}$	-241.6		
[F-**1**]$^•$	-75.2	**1**$^{•+}$ / [F-**1**]$^•$	**277.2** (FIA)
[F₂-**1**]$^{-•}$	-210.9	[F-**1**]$^•$ / [F₂-**1**]$^{-•}$	**124.6** (FIA)

Table S6. Computed data for the calculation of ²⁹Si NMR resonances.

Compound	Isotropic Shielding	Solvent	Resonance δ [ppm]
Si(CH₃)₄ $^{[a]}$	332.45	CH₂Cl₂	0.0
Si(CH₃)₄ $^{[b]}$	332.13	CH₂Cl₂	0.0
Si(cat$^{3,4,6-iPr}$)₂ $^{[a]}$	371.22	CH₂Cl₂	−38.8
[Si(cat$^{3,4,6-iPr}$)₂]₂ $^{[a]}$	405.15	CH₂Cl₂	−72.7
	398.58		−66.1
Si(cat$^{3,5-Cm}$)₂ $^{[a]}$	371.37	CH₂Cl₂	−38.9
[Si(cat$^{3,5-Cm}$)₂]₂ $^{[b]}$	401.29	CH₂Cl₂	−69.2
	406.39		−74.3
1 $^{[a]}$	371.37	CH₂Cl₂	−38.9
[**1**]₂ $^{[a]}$	410.92	CH₂Cl₂	−78.5
	410.39		−77.9

Calculation of the NMR resonances at the PBE0-D3(BJ)+SMD(*solvent*)/def2-TZVPP level of theory. Optimization level: [a] PBEh-3c (*Orca 5.0*) [b] Opt. PBEh-3c (*Orca 4.2*).

Table S7. Computed energies and thermodynamic data for the dimerization of alkylated bis(catecholato)silanes. ΔG energies were referenced against 2 equivalents of the respective monomeric unit.

Compound	E^{OPT} [H]	G^{OPT} [H]	H^{OPT} [H]	E^{SP} [H]	G [kJ mol^{-1}]	ΔG [kJ mol^{-1}]
1	-1678.3346	-1677.7441	-1677.6512	-1680.5223	-4410653.7	**0.0**
TS-[**1**]$_2$‡	-3356.6703	-3355.4549	-3355.3020	-3361.0422	-8821218.1	**89.2**
[**1**]$_2$	-3356.6860	-3355.4752	-3355.3172	-3361.0637	-8821286.5	**20.8**
Si(cat$^{3,4,6\text{-}iPr}$)$_2$	-1756.7974	-1756.1537	-1756.0513	-1759.0875	-4616786.6	**0.0**
TS-[Si(cat$^{3,4,6\text{-}iPr}$)$_2$]$_2$‡	-3513.5914	-3512.2695	-3512.0976	-3518.1673	-9233470.2	**103.0**
[Si(cat$^{3,4,6\text{-}iPr}$)$_2$]$_2$	-3513.6100	-3512.2914	-3512.1163	-3518.1777	-9233517.4	**55.8**
Si(cat$^{3,5\text{-}Cm}$)$_2$	-2443.5766	-2442.7805	-2442.6625	-2446.9056	-6422253.0	**0.0**
TS-[Si(cat$^{3,5\text{-}Cm}$)$_2$]$_2$‡	-4887.1676	-4885.5414	-4885.3393	-4893.8233	-12844467.7	**38.4**
[Si(cat$^{3,5\text{-}Cm}$)$_2$]$_2$	-4887.2103	-4885.5857	-4885.3802	-4893.8644	-12844568.8	**62.5**

DSD-BLYP-D3(BJ)/def2-QZVPP+SMD(CH$_2$Cl$_2$)//PBEh-3c level of theory (*Orca 5.0*).

Table S8. Computed energies and thermodynamic data for the adduct formation of **1** and N(p-C$_6$H$_4$Br)$_3$.

Compound	E^{OPT} [H]	G^{OPT} [H]	H^{OPT} [H]	E^{SP} [H]	G [kJ mol^{-1}]	ΔG [kJ mol^{-1}]
1	-1681.1118	-1680.5525	-1680.4554	-1684.0960	-4420117.8	**0.0**
N(p-C$_6$H$_4$Br)$_3$	-8470.1536	-8469.9569	-8469.8874	-8475.0916	-22250830.3	
1-N(p-C$_6$H$_4$Br)$_3$	-10151.2939	-10150.5024	-10150.3670	-10159.2117	-26670926.2	**21.9**

PW6B95-D4/def2-TZVPP+SMD(CH$_2$Cl$_2$)//r^{2}SCAN-3c+CPCM(CH$_2$Cl$_2$) level of theory (*Orca 5.0*).

FIA Data shown in Figure 3 of the Manuscript

Table S9. Literature data for the FIAs shown in Figure 3 of the main manuscript.

Compound	Level of theory	Reference	FIA [kJ mol^{-1}]
Me$_3$Si$^+$	*CCSD(T)/CBS (serves as anchor point)*	[53]	**953**
[P(am$^\Gamma$ph$^\Gamma$)$_2$]$^+$)	*DLPNO-CCSD(T)/def2-TZVPP//ωB97X-D3(BJ)/def2-TZVPP*	[10]	**825**
1$^{•+}$	*DLPNO-CCSD(T)/def2-QZVPP//PBE0-D3(BJ)/def2-TZVP*	*this work*	**784**
[FP(C$_6$F$_5$)$_3$]$^+$	*DLPNO-CCSD(T)/def2-TZVPP//ωB97X-D3(BJ)/def2-TZVPP*	[10]	**717**
1	*DLPNO-CCSD(T)/def2-QZVPP//PBE0-D3(BJ)/def2-TZVP*	*this work*	**404**

6. Single Crystal X-Ray Diffraction (scXRD)

A colorless, block-shaped crystal was mounted on a MiTeGen micromount with perfluoroether oil. Data were collected from a shock-cooled single crystal at 100(2) K on a Bruker D8 VENTURE dual wavelength Mo/Cu four-circle diffractometer with a microfocus sealed X-ray tube using a mirror optics as monochromator and a Bruker PHOTON III detector. The diffractometer was equipped with an Oxford Cryostream 700 low temperature device and used MoK_{α} radiation (λ = 0.71073 Å). All data were integrated with SAINT V8.40B and a multi-scan absorption correction using SADABS 2016/2 was applied.[63, 64] The structure was solved by direct methods with SHELXT and refined by full-matrix least-squares methods against F^2 using SHELXL-2019/2.[65, 66] All non-hydrogen atoms were refined with anisotropic displacement parameters. All hydrogen atoms were refined isotropic on calculated positions using a riding model with their U_{iso} values constrained to 1.5 times the U_{eq} of their pivot atoms for terminal sp^3 carbon atoms and 1.2 times for all other carbon atoms.

Crystallographic data for the structures reported in this paper have been deposited with the Cambridge Crystallographic Data Centre.[67] CCDC 2402241 contains the supplementary crystallographic data for this paper. These data can be obtained free of charge from the *Cambridge Crystallographic Data Centre via* www.ccdc.cam.ac.uk/structures. This report and the CIF file were generated using FinalCif.[68]

For data visualization, Mercury 4.1.3 was used.[69-71] The thermal displacement ellipsoids are shown at the probability level of 50%.
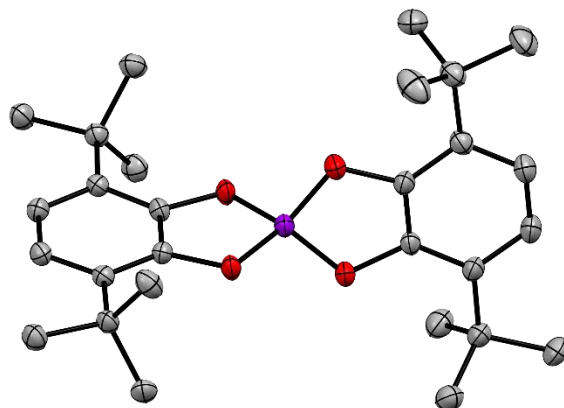
Figure S3. Solid state molecular structure of 1. Ellipsoids are drawn with a probability of 50%. Hydrogen atoms are omitted for clarity.

Table S10. Crystal data for **1**.

|	
CCDC number	2402241
Empirical formula	$C_{28}H_{40}O_4Si$
Formula weight	468.69
Temperature [K]	100(2)
Crystal system	monoclinic
Space group (number)	$P2_1/c$ (14)
a [Å]	13.651(4)
b [Å]	18.181(5)
c [Å]	11.1582(19)
α [°]	90
β [°]	101.590(11)
γ [°]	90
Volume [Å^3]	2712.8(12)
Z	4
ρ_{calc} [gcm^{-3}]	1.148
μ [mm^{-1}]	0.116
$F(000)$	1016
Crystal size [mm^3]	0.05×0.09×0.11
Crystal color	colourless
Crystal shape	block
Radiation	MoK_α (λ=0.71073 Å)
2θ range [°]	4.35 to 54.57 (0.78 Å)
Index ranges	−17 ≤ h ≤ 17
	−23 ≤ k ≤ 23
	0 ≤ l ≤ 14
Reflections collected	6020
Independent reflections	6020
	R_{int} = 0.0683
	R_{sigma} = 0.0502
Completeness to θ = 25.242°	99.7 %
Data / Restraints / Parameters	6020 / 0 / 311
Goodness-of-fit on F^2	0.6683 / 0.7455 (multi-scan)
Final R indexes [$I{\geq}2\sigma(I)$]	1.067
Final R indexes [all data]	R_1 = 0.0617
	wR_2 = 0.1627
Largest peak/hole [eÅ^{-3}]	R_1 = 0.0778
	wR_2 = 0.1797

7. References

1   I. Belostotskaya, N. Komissarova, E. Dzhuaryan and V. Ershov, *Bull. Acad. Sci. USSR, Div. Chem. Sci.*, 1972, **21**, 1535-1536.
2   J. M. Schümann, J. P. Wagner, A. K. Eckhardt*, et al.*, *J. Am. Chem. Soc.*, 2021, **143**, 41-45.
3   D. E. Wheeler and J. K. McCusker, *Inorg. Chem.*, 1998, **37**, 2296-2307.
4   J. J. Adams, N. Arulsamy, B. P. Sullivan*, et al.*, *Inorg. Chem.*, 2015, **54**, 11136-11149.
5   K. U. Ingold, *Can. J. Chem.*, 1963, **41**, 2807-2815.
6   J. J. Conradi and G. A. McLaren, *J. Am. Chem. Soc.*, 1960, **82**, 4745-4745.
7   R. Maskey, T. Thorwart, S. F. Ebel*, et al.*, *Chem. Eur. J.*, 2023, **29**, e202300269.
8   M. Bamberg, M. Bursch, A. Hansen*, et al.*, *J. Am. Chem. Soc.*, 2021, **143**, 10865-10871.
9   D. Hartmann, T. Thorwart, R. Müller*, et al.*, *J. Am. Chem. Soc.*, 2021, **143**, 18784-18793.
10   D. Roth, J. Stirn, D. W. Stephan and L. Greb, *J. Am. Chem. Soc.*, 2021, **143**, 15845-15851.
11   M. Mehta, M. H. Holthausen, I. Mallov*, et al.*, *Angew. Chem. Int. Ed.*, 2015, **54**, 8250-8254.
12   T. Thorwart, D. Roth and L. Greb, *Chem. Eur. J.*, 2021, **27**, 10422-10427.
13   D. Roth, H. Wadepohl and L. Greb, *Angew. Chem. Int. Ed.*, 2020.
14   F. Neese, *Wiley Interdiscip. Rev. Comput. Mol. Sci.*, 2012, **2**, 73-78.
15   F. Neese, *Wiley Interdiscip. Rev. Comput. Mol. Sci.*, 2018, **8**, e1327.
16   S. Grimme, C. Bannwarth and P. Shushkov, *J. Chem. Theory Comput.*, 2017, **13**, 1989-2009.
17   C. Bannwarth, S. Ehlert and S. Grimme, *J. Chem. Theory Comput.*, 2019, **15**, 1652-1671.
18   C. Bannwarth, E. Caldeweyher, S. Ehlert*, et al.*, *Wiley Interdiscip. Rev. Comput. Mol. Sci.*, 2021, **11**, e1493.
19   M. D. Hanwell, D. E. Curtis, D. C. Lonie*, et al.*, *J. Cheminform.*, 2012, **4**, 17.
20   P. Pracht, F. Bohle and S. Grimme, *Phys. Chem. Chem. Phys.*, 2020, **22**, 7169-7192.
21   K. Eichkorn, O. Treutler, H. Öhm*, et al.*, *Chem. Phys. Lett.*, 1995, **242**, 652-660.
22   F. Neese, F. Wennmohs, A. Hansen and U. Becker, *Chem. Phys.*, 2009, **356**, 98-109.
23   K. Eichkorn, F. Weigend, O. Treutler and R. Ahlrichs, *Theor. Chem. Acc.*, 1997, **97**, 119-124.
24   A. D. Becke and E. R. Johnson, *J. Chem. Phys.*, 2005, **123**, 154101.
25   A. D. Becke and E. R. Johnson, *J. Chem. Phys.*, 2005, **122**, 154104.
26   S. Grimme, J. Antony, S. Ehrlich and H. Krieg, *J. Chem. Phys.*, 2010, **132**, 154104.
27   S. Grimme, S. Ehrlich and L. Goerigk, *J. Comput. Chem.*, 2011, **32**, 1456-1465.
28   E. Caldeweyher, S. Ehlert, A. Hansen*, et al.*, *J. Chem. Phys.*, 2019, **150**.
29   S. Grimme, J. G. Brandenburg, C. Bannwarth and A. Hansen, *J. Chem. Phys.*, 2015, **143**, 054107.
30   S. Grimme, A. Hansen, S. Ehlert and J.-M. Mewes, *J. Chem. Phys.*, 2021, **154**, 064103
31   J. P. Perdew, K. Burke and M. Ernzerhof, *Phys. Rev. Lett.*, 1996, **77**, 3865-3868.
32   C. Adamo and V. Barone, *J. Chem. Phys.*, 1999, **110**, 6158-6170.
33   Y. Zhao and D. G. Truhlar, *J. Phys. Chem. A*, 2005, **109**, 5656-5667.
34   S. Kozuch, D. Gruzman and J. M. Martin, *J. Phys. Chem. C*, 2010, **114**, 20801-20808.

35   A. Schäfer, C. Huber and R. Ahlrichs, *J. Chem. Phys.*, 1994, **100**, 5829-5835.
36   F. Weigend and R. Ahlrichs, *Phys. Chem. Chem. Phys.*, 2005, **7**, 3297-3305.
37   A. K. Wilson, D. E. Woon, K. A. Peterson and T. H. Dunning Jr., *J. Chem. Phys.*, 1999, **110**, 7667-7676.
38   N. B. Balabanov and K. A. Peterson, *J. Chem. Phys.*, 2006, **125**, 074110.
39   N. B. Balabanov and K. A. Peterson, *J. Chem. Phys.*, 2005, **123**, 064107.
40   D. E. Woon and T. H. Dunning Jr., *J. Chem. Phys.*, 1993, **98**, 1358-1371.
41   B. P. Prascher, D. E. Woon, K. A. Peterson*, et al.*, *Theor. Chem. Acc.*, 2011, **128**, 69-82.
42   R. A. Kendall, T. H. Dunning Jr. and R. J. Harrison, *J. Chem. Phys.*, 1992, **96**, 6796-6806.
43   F. Neese, A. Hansen and D. G. Liakos, *J. Chem. Phys.*, 2009, **131**, 064103.
44   C. Riplinger and F. Neese, *J. Chem. Phys.*, 2013, **138**, 034106.
45   C. Riplinger, B. Sandhoefer, A. Hansen and F. Neese, *J. Chem. Phys.*, 2013, **139**, 134101.
46   S. Ehlert, M. Stahn, S. Spicher and S. Grimme, *J. Chem. Theory Comput.*, 2021, **17**, 4250-4261.
47   A. V. Marenich, C. J. Cramer and D. G. Truhlar, *J. Phys. Chem. B*, 2009, **113**, 6378-6396.
48   C. J. Cramer, *Essentials of computational chemistry: theories and models*, John Wiley & Sons, 2013.
49   S. Grimme, *Chem. Eur. J.*, 2012, **18**, 9955-9964.
50   G. A. Andrienko, *https://www.chemcraftprog.com*, ChemCraft 1.8.
51   H. Böhrer, N. Trapp, D. Himmel*, et al.*, *Dalton Trans.*, 2015, **44**, 7489-7499.
52   L. O. Müller, D. Himmel, J. Stauffer*, et al.*, *Angew. Chem. Int. Ed.*, 2008, **47**, 7659-7663.
53   P. Erdmann, J. Leitner, J. Schwarz and L. Greb, *ChemPhysChem*, 2020, **21**, 987-994.
54   P. Erdmann and L. Greb, *ChemPhysChem*, 2021, **22**, 935-943.
55   C. C. Pye and T. Ziegler, *Theor. Chem. Acc.*, 1999, **101**, 396-408.
56   G. te Velde, F. M. Bickelhaupt, E. J. Baerends*, et al.*, *J. Comput. Chem.*, 2001, **22**, 931-967.
57   E. Van Lenthe and E. J. Baerends, *J. Comput. Chem.*, 2003, **24**, 1142-1156.
58   F. Eckert and A. Klamt, *AIChE J.*, 2002, **48**, 369-385.
59   A. Klamt and M. Diedenhofen, *J. Comput. Aided Mol. Des.*, 2010, **24**, 357-360.
60   A. Klamt, *J. Phys. Chem.*, 1995, **99**, 2224-2235.
61   A. Klamt, B. Mennucci, J. Tomasi*, et al.*, *Acc. Chem. Res.*, 2009, **42**, 489-492.
62   M. Bursch, T. Gasevic, J. B. Stückrath and S. Grimme, *Inorg. Chem.*, 2021, **60**, 272-285.
63   Bruker, *SAINT, V8.40B*, **Bruker AXS Inc., Madison, Wisconsin, USA**.
64   L. Krause, R. Herbst-Irmer, G. M. Sheldrick and D. Stalke, *J. Appl. Crystallogr.*, 2015, **48**, 3-10.
65   G. Sheldrick, *Acta Crystallogr. A*, 2015, **A71**, 3-8.
66   G. Sheldrick, *Acta Crystallogr. C*, 2015, **C71**, 3-8.
67   C. R. Groom, I. J. Bruno, M. P. Lightfoot and S. C. Ward, *Acta Crystallogr. B*, 2016, **B72**, 171-179.
68   D. Kratzert, *FinalCif*, **V143**, https://dkratzert.de/finalcif.html.
69   I. J. Bruno, J. C. Cole, P. R. Edgington*, et al.*, *Acta Crystallogr. B*, 2002, **58**, 389-397.
70   C. F. Macrae, P. R. Edgington, P. McCabe*, et al.*, *J. Appl. Crystallogr.*, 2006, **39**, 453-457.
71   C. F. Macrae, I. Sovago, S. J. Cottrell*, et al.*, *J. Appl. Crystallogr.*, 2020, **53**, 226-235.

8. EPR Simulation Data, Spectra and Voltammograms

Table S11. Parameters for the experiment and the simulation of the EPR spectrum of **1•+**.

Experiment parameter	Value
Frequency	9.450515 GHz
Solvent	$o\text{-}C_6H_4F_2$

Simulation parameter	Value
Field center	337.300
Domain	CW
Rel. conc.	100.000
Line width	0.380
Lorentzian	15.000
g-shift	−0.145
Nuclei	2
Coupling	0.716
Spin	0.5
g value	$g = \dfrac{h \bullet 9.450515\ GHz}{\mu_B \bullet 337.155\ mT} = 2.00269$
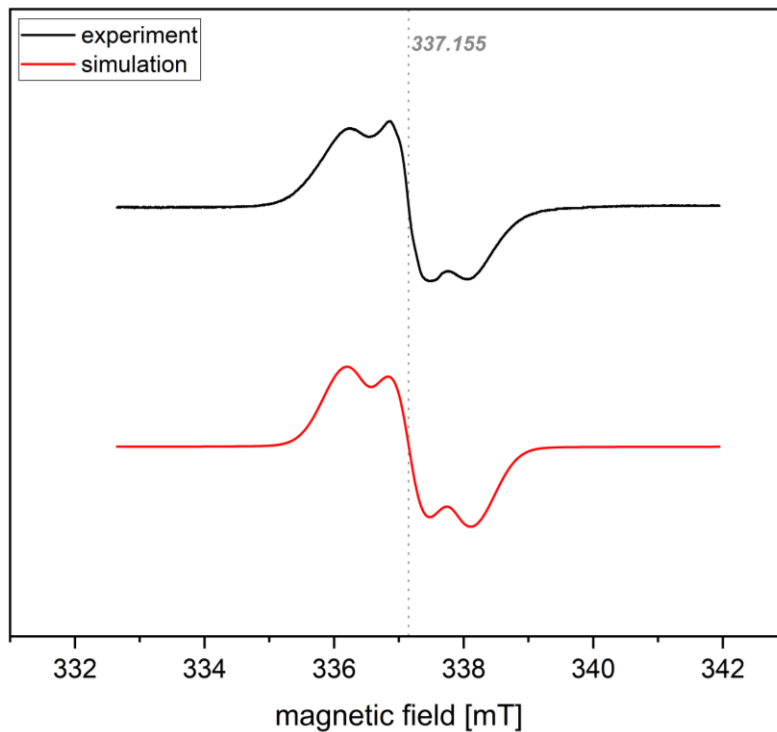
Figure S4. Stacked EPR spectra from experiment ([**1**][B(C₆F₅)₄] in $o\text{-}C_6H_4F_2$) and simulation (**1•+**). Pearson correlation 99.3% as determined by the *winsim* program package.
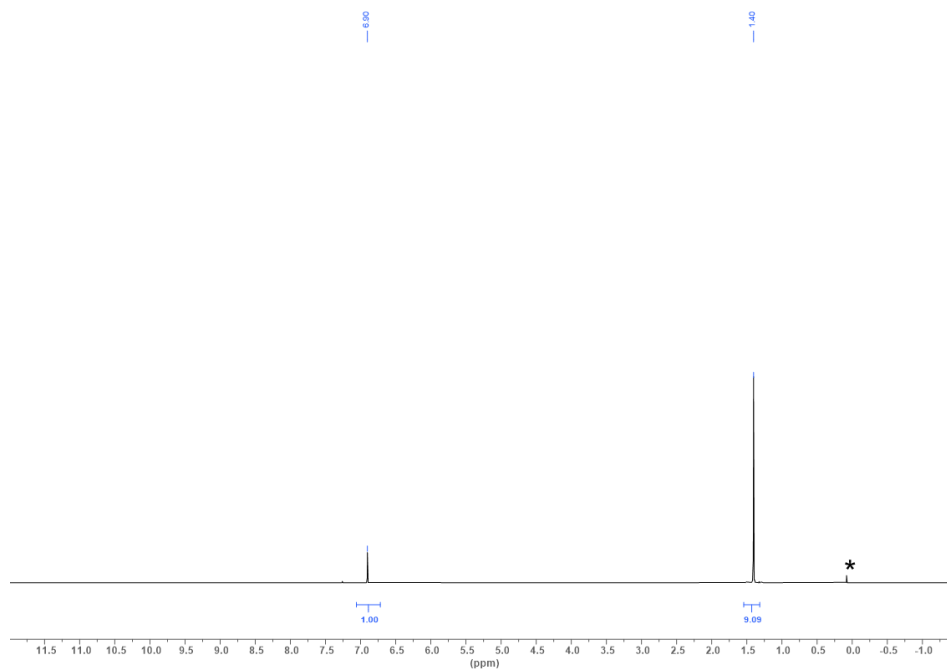
Figure S5. ¹H NMR spectrum of **1**. Silicone-grease impurity originating from the NMR-solvent is marked with an asterisk (*).
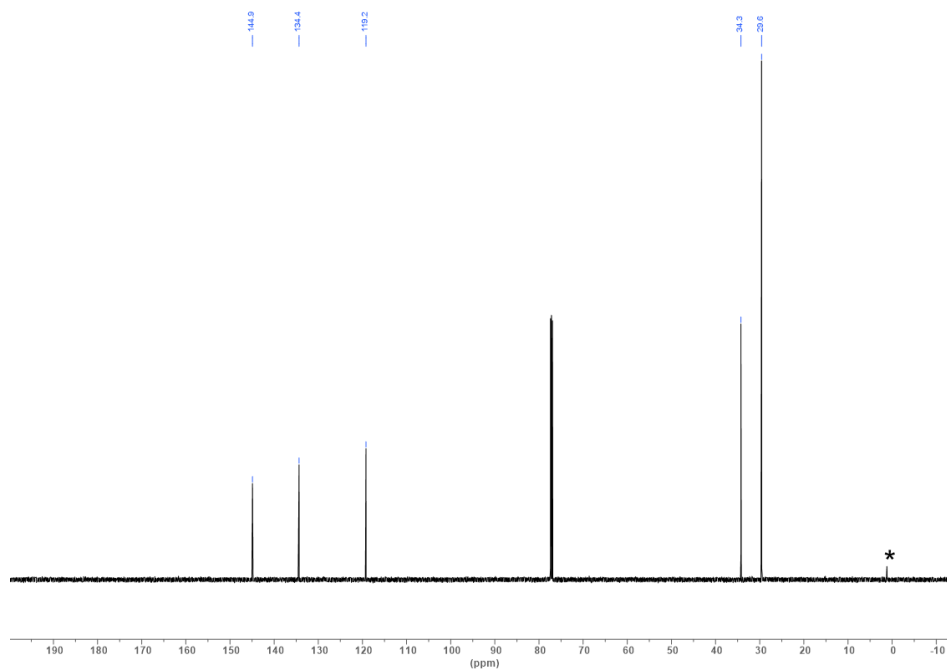
Figure S6. ¹³C NMR spectrum of **1**. Silicone-grease impurity originating from the NMR-solvent is marked with an asterisk (*).

—42.9
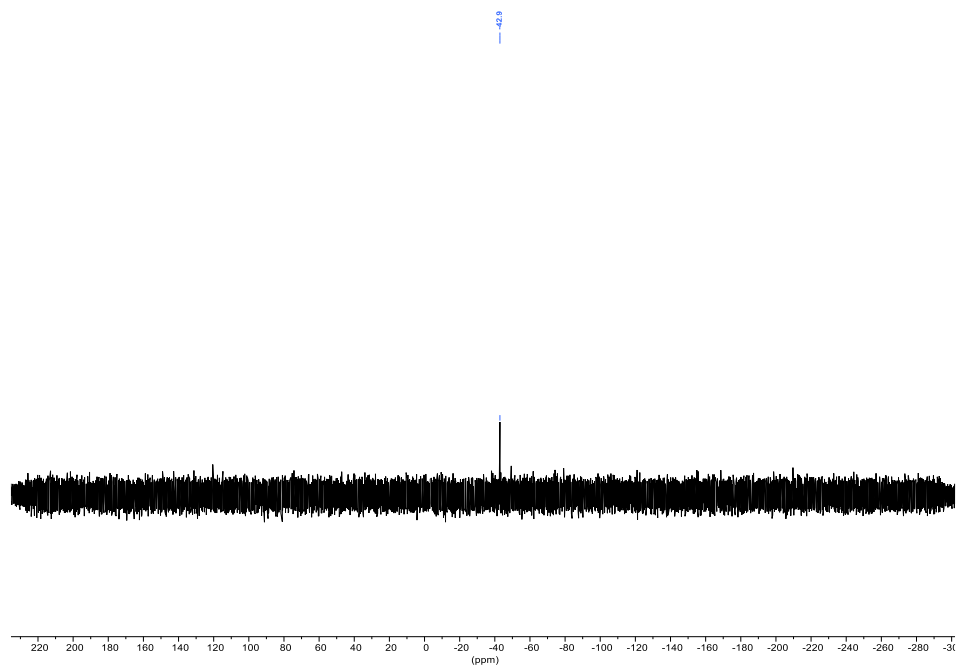
Figure S7. ^{29}Si NMR spectrum of **1**.

—1.16
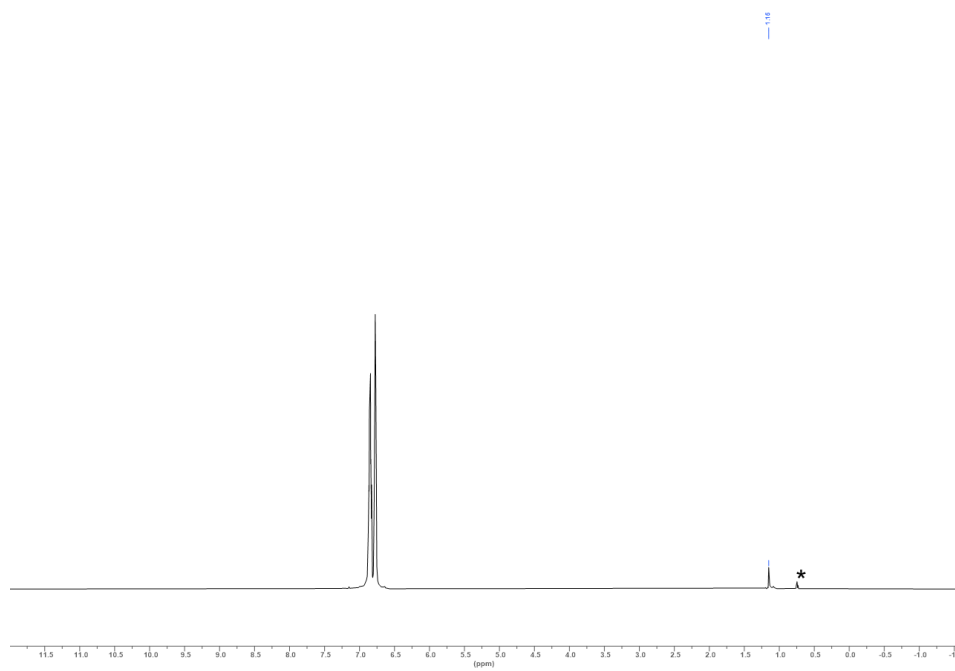
Figure S8. ^{1}H NMR spectrum of **[1]**[B(C$_6$F$_5$)$_4$]. Signal of residual *n*-hexane is marked with an asterisk (*).
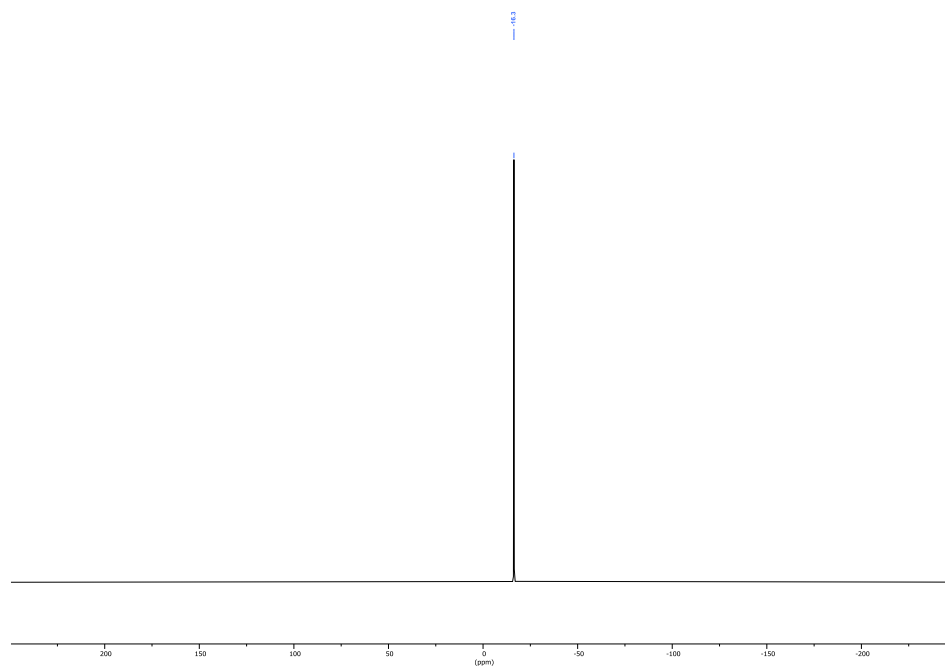
Figure S9. ^{11}B NMR spectrum of **[1]**[B(C$_6$F$_5$)$_4$].
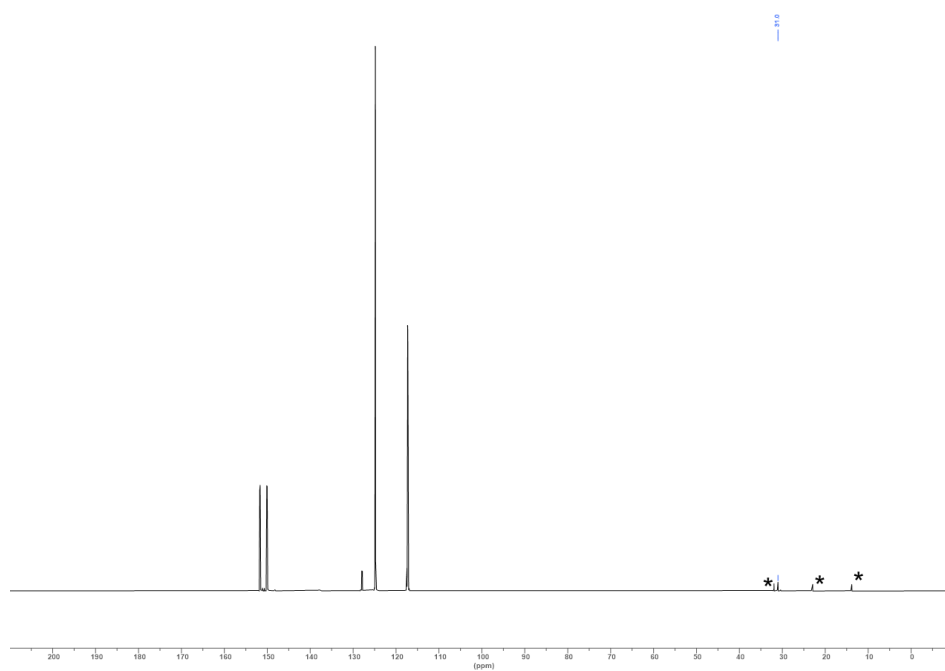
Figure S10. ^{13}C NMR spectrum of **[1]**[B(C$_6$F$_5$)$_4$]. Signals of residual *n*-hexane are marked with an asterisk (*).
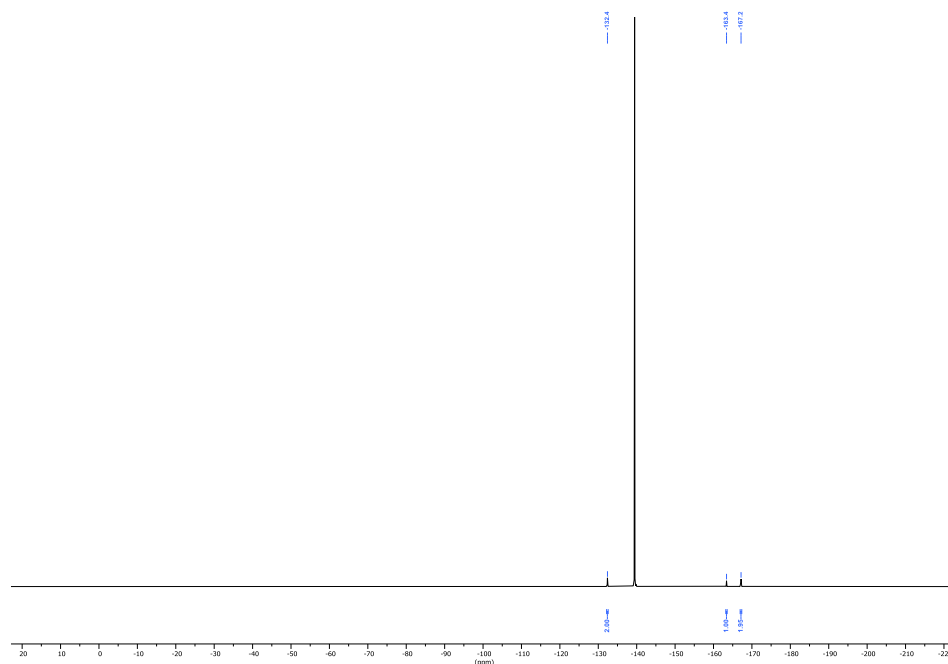
Figure S11. ¹⁹F NMR spectrum of **[1]**[B(C₆F₅)₄].
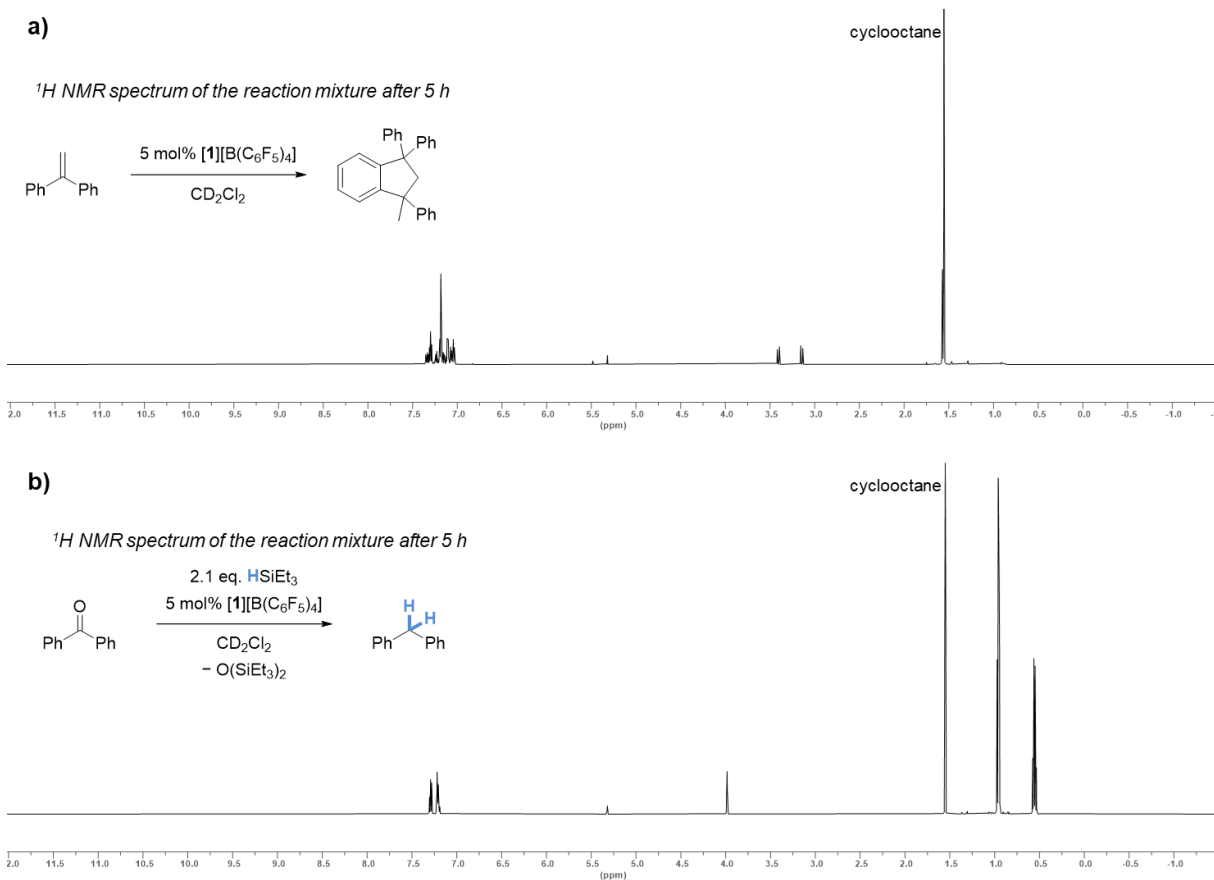
Figure S12. ¹H NMR spectra (600 MHz, in CD₂Cl₂) of the reaction mixtures of the **[1]**[B(C₆F₅)₄] catalyzed a) Friedel-Craft's Dimerization and b) dihydrodeoxygenation of benzophenone.
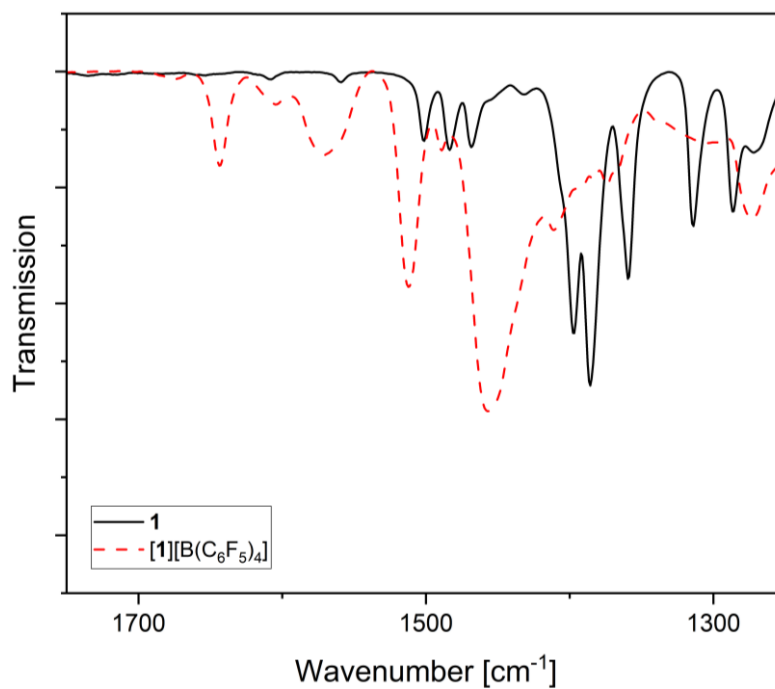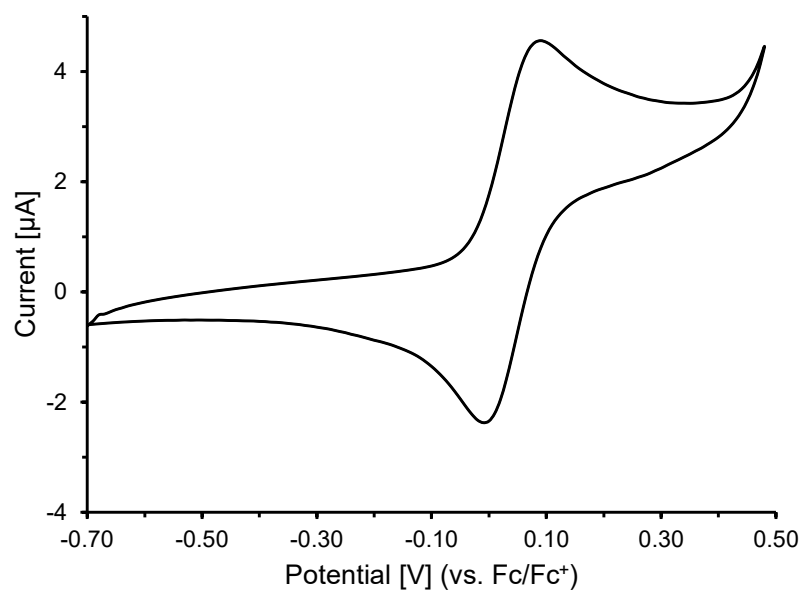
Figure S13. Comparison of IR spectra of **1** and **[1]**[B(C₆F₅)₄] in the area of C-O modes.
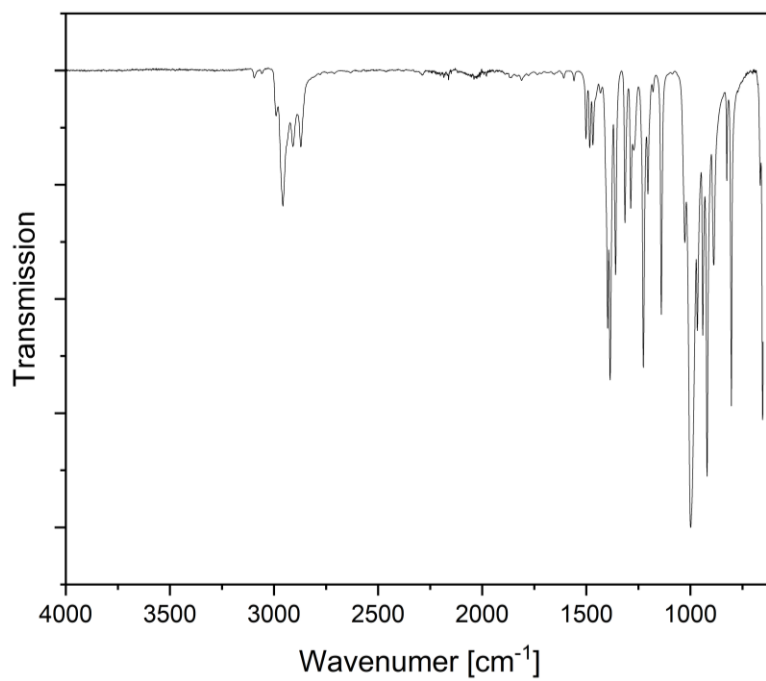
Figure S14. ATR-IR absorption spectrum of **1**. The spectrum was manually base-line corrected after data acquisition.
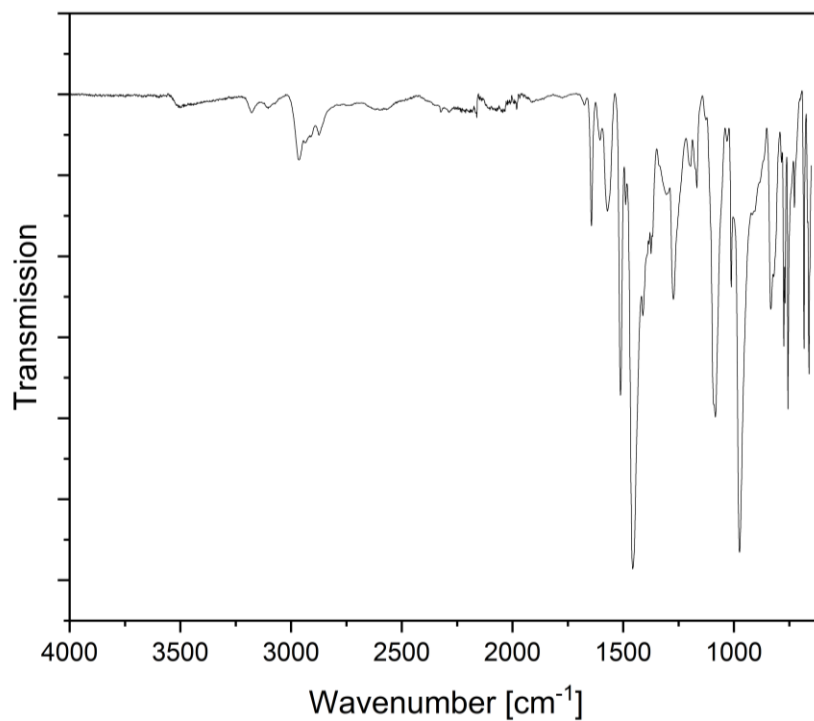
Figure S15. ATR-IR absorption spectrum of [**1**][B(C$_6$F$_5$)$_4$]. The spectrum was manually base-line corrected after data acquisition.

Figure S16. Cyclic voltammogram of **1** in dichloromethane ([N^{n}Bu$_4$][PF$_6$], 50 mV/s).